Localization dynamics in the Creutz-Hubbard ladder
A GEFES Research Awards Report

Student: Juan Zurita Alonso Tutor: Charles Creffield

Departamento de Física de Materiales, Universidad Complutense de Madrid

Our work consisted on an analytical and numerical study of the localization dynamics, topology and interaction effects in the bosonic Creutz-Hubbard ladder model, and its possible implementation in a photonic waveguide lattice setup. To that end, we first considered the non-interacting Creutz ladder, interesting because of its non-trivial topology and extreme self-localization phenomena, and recently realized experimentally in a cold atom lattice. The work this document is a report on has been published at [1] in an open access regime.

This work has been realized in close collaboration with Professor Gloria Platero at ICMM-CSIC.

1 Introduction

Recent years have seen vast advances in the field of quantum simulation, an approach first proposed by Feynman, [2] in which the dynamics of some complicated quantum system is simulated by another,highly-controllable, quantum system. In principle, this technique can provide an enormous speed advantage over the conventional approach of simulating such systems using classical computers, a feature known as "quantum supremacy". [3] A particularly important application of quantum simulation is the investigation of topological insulators; materials which are insulating in the bulk, but possess conductive surface states protected by topological order.

In this paper, we first study the effects of AB interference on one-particle states in a particular topological insulator, the Creutz ladder, and show how they can be observed experimentally in a photonic waveguide lattice. We then proceed to investigate how interactions modify these results, by introducing the minimal model which incorporates interparticle interactions: the two-particle Creutz-Hubbard ladder. Finally, we propose a way to implement the latter model in a photonic waveguide system, focusing on the geometry of the lattice and the necessary use of synthetic dimensions. [4]

2 Creutz ladder

The Creutz ladder (Figure 1a) [5] consists of two chains of sites connected with horizontal, vertical and diagonal hopping amplitudes. Additionally, a magnetic field is applied perpendicularly to the plane of the ladder. This causes some hopping amplitudes to acquire a so-called Peierls phase and become complex. We choose the gauge in which the horizontal hoppings cause a change of phase of $e^{\pm i\phi/2}$ in the wavefunction, and the rest are real. The sign of the phase change is positive if the particle moves to the right (left) on the upper (lower) leg of the ladder, and negative if it moves in the opposite direction. For $m = 0$ (no "rung" hopping terms), the lattice is bipartite, given that all first neighbours of sites with an odd j-coordinate correspond to an even j, and vice versa.

We will first consider the single-particle case, and go on to consider interactions in Sec. 3. Let $c^{(\dagger)}_{j,\alpha}$ be the destruction (creation) operator for a boson in site $|j,\alpha\rangle$ of the ladder, where $j = 1,...,L$ labels the rungs along the ladder and $\alpha = A,B$ labels the two legs. The Creutz Hamiltonian then takes the form:

$$\mathscr{H}_C = -\sum_{j,\alpha}\Big[J_\alpha c^\dagger_{j+1,\alpha}c_{j,\alpha} + J c^\dagger_{j+1,\alpha}c_{j,\overline{\alpha}} + \\ + \frac{m}{2}c^\dagger_{j,\alpha}c_{j,\overline{\alpha}} + H.c.\Big] \quad (1)$$

where the horizontal hopping terms are $J_\alpha = Je^{i\sigma_\alpha\phi/2}$, with $\sigma_{A/B} = \pm 1$ and $\overline{A} = B$ and vice versa. The model is thus specified by two hopping amplitudes (J and m), and the magnetic flux, represented by ϕ.

The physical magnetic flux that threads each plaquette, Φ, is proportional to the total phase ϕ acquired by a particle moving along its border in a clockwise sense. The Hamiltonian can be written in momentum space in terms of the Pauli matrices as $\mathscr{H}(k) = d_0\mathbb{1} + \vec{d}\cdot\vec{\sigma}$, with $d_y = 0$. In the abstract space formed by $\vec{d} = (d_z, d_x, d_0)$, the d_0 axis corresponds to the possible band degeneracies (i.e. gap closings) in the bands of the Creutz Hamiltonian. This means that, for an insulating system, the winding number of its closed directed

path $\tilde{d}(k)$ around the d_0 axis determines the topological invariant of the Hamiltonian, of type $\mathbb{Z}$, which serves to distinguish the different topological phases of the system. In Figure 1c, all paths have been projected down to the $(d_z(k), d_x(k))$ plane for simplicity.

We show the topological phase diagram of the system as a function of the phase induced by the magnetic flux, ϕ, and the vertical hopping amplitude, m, in Figure 1b. [6] Four topological phases can be distinguished. The system is topologically trivial for $|m| > 2J$, with a vanishing winding number, and thus a Zak phase of zero. For $|m| < 2J$, two different topological phases exist, with winding numbers of $\nu = \pm 1$, depending on the value of ϕ. Both phases are associated with a Zak phase of $= \pi$, given that this quantity is defined modulo 2π. The boundaries of these regions correspond to metallic systems, in which the two bands of the model touch. The phase diagram is periodic in ϕ, with period 4π. This means that the left and right sides of Figure 1b represent the same points in phase space. As a simple consistency check, we calculated the Zak phase numerically for different points of the phase space.

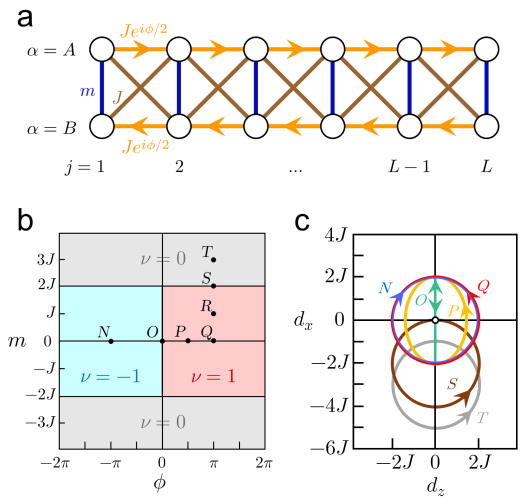

Figure 1: a) Geometry of the Creutz ladder. All parameters are defined in the main text. b) Topological phase diagram for the Creutz ladder. The left and right edges of the diagram represent the same systems. Two trivial ($\nu = 0$) and two nontrivial ($\nu = \pm 1$) topological phases can be distinguished. c) Image of the function $(d_x(k), d_z(k))$ along the Brillouin zone for some of the points in the phase diagram. Its winding number around the origin corresponds to the topological invariant ν of the phase the point belongs to.

3 Creutz-Hubbard ladder

As we noted earlier, interactions between particles play an interesting role in both topological and flat band systems. This motivates the inclusion of an interaction term in the Creutz Hamiltonian. In the literature, nearest neighbor [7–9] or on-site interactions, both attractive [10, 11] and repulsive [12, 13] have been considered, We will consider an on-site repulsive ($U > 0$) Hubbard interaction term in the Creutz Hamiltonian:

$$\mathcal{H}_{CH} = \mathcal{H}_C + \frac{U}{2}\sum_{j,\alpha} c^\dagger_{j\alpha} c^\dagger_{j\alpha} c_{j\alpha} c_{j\alpha}. \tag{2}$$

Given that $c^{(\dagger)}_{j\alpha}$ are bosonic operators, there is no limit to the number of particles that a single site can hold. Nevertheless, for reasons that will become apparent soon, we will focus on the case where only two particles populate the ladder, the minimal case for interaction effects to occur. We are able to do this because the Creutz-Hubbard Hamiltonian preserves the number of particles. Additionally, its correlated nature prevents the use of a single-particle approach. We will use a bosonic Fock space basis $\{|1_{i,\alpha} 1_{j,\beta}\rangle\}_{i,\alpha,j,\beta}$.

3.1 Effective Hamiltonian, doublon caging and edge states

For sufficiently large values of U, the repulsive interaction can actually bind both particles together. This can be understood in energetic terms: if $U \gg J, m$, the states of the system with a doubly-occupied site have a much higher energy than the others. Conservation of energy means that a doubly occupied state cannot evolve into a pair of separated particles under time evolution. Both particles thus move together around the lattice as a pair, forming a *doublon*. Thus, a doublon is a quasiparticle composed of two particles which are bound as a result of a repulsive Hubbard interaction, in which both particles occupy the same site.
The fact that the doublon bands (formed by all the doubly occupied states of the Fock basis) are decoupled from the rest of the spectrum (the singly occupied states) can be exploited to execute a Schrieffer-Wolff transformation and obtain an effective Hamiltonian for the doublon subspace. [14–16] The resulting

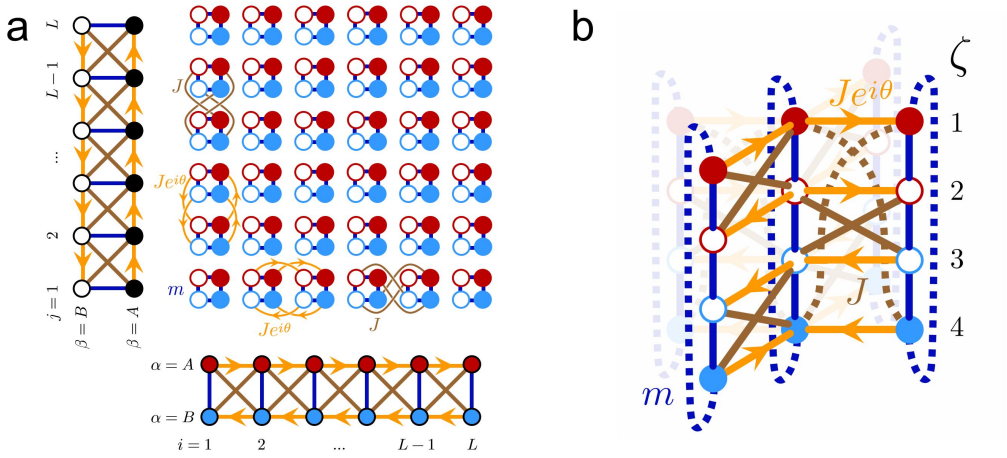

Figure 2: a) Quasi-2D lattice for the effective model, result of the Cartesian product of two Creutz ladders (left and bottom). All of the intercell (orange and brown) hoppings in the figure must be established between all adjacent unit cells. b) Portion of the analogous lattice in 3D. The three nonlocal hoppings per unit cell are represented by dotted lines.

Hamiltonian, for a finite system, takes the form:

$$\begin{aligned}\mathscr{H}_{\text{eff}} = &\sum_{j,\alpha}\Big[\frac{J_\alpha^2}{U}d^\dagger_{j+1,\alpha}d_{j,\alpha} + \frac{J^2}{U}d^\dagger_{j+1,\alpha}d_{j,\bar{\alpha}} + \\ &+ \frac{m^2}{2U}d^\dagger_{j,\alpha}d_{j,\bar{\alpha}} + H.c.\Big] + \frac{U}{2}\sum_{j,\alpha}d^\dagger_{j\alpha}d_{j\alpha} + \\ &- \sum_{\alpha}\mu[d^\dagger_{1\alpha}d_{1\alpha} + d^\dagger_{L\alpha}d_{L\alpha}] + \Delta \end{aligned} \tag{3}$$

where $d^{(\dagger)}_{j\alpha} \equiv (c^{(\dagger)}_{j\alpha})^2$ are the doublon creation and annihilation operators, and $\Delta = [(2m^2 + 8J^2)/U]\mathbb{1}$ is an energy offset of the whole Hamiltonian with respect to the original scale of energy. The first sum is a renormalized Creutz model, with $-J \to J^2/U$, $-J_\alpha \to J_\alpha^2/U$, $-m \to m^2/U$. The second term is the Hubbard interaction term, which remains unchanged. Additionally, a chemical potential $-\mu = -2J^2/U$ appears in the end sites, because of their different coordination number than the rest of the lattice. This same phenomenon was demonstrated in other 1D and 2D effective models for doublons. [16, 17]

Given that the doublon will have an electric charge $2q$ (with q the charge of one particle), we can expect to find analogues of the behaviour found in the single particle dynamics for half the magnetic flux than in the latter case. In particular, AB caging for doublons is expected to be found for $\phi = \pm\pi/2$. Because of the periodicity of the phase diagram in ϕ, caging should also be found for $\phi = \pm 3\pi/2$. For these values of the flux, the independent particles are not localized, and this paints an interesting picture: an ensemble of localized doublons and free-moving particles. This is the opposite situation to the rungless π-flux regime, in which particles were caged and pairs could propagate. The behaviour for $m \neq 0$ is analogous to the single-particle case: including a vertical hopping amplitude breaks AB caging for all values of ϕ. In the following, we will focus on the case with $m = 0$.

Doublon edge states, which have been studied for different 1D and 2D systems [16–19], cannot be treated in the same way as their single particle counterparts in 1D and quasi-1D systems, as the usual bulk-boundary correspondence is not valid and the value of the Zak phase is not correlated to the existence of topological doublon edge states. [18] Consequently a different approach must be employed. In the $m = 0$ case, the simplicity of the AB-localized single-particle edge states allows us to probe for analogous doublon edge states. The relative phase between the sites must now be twice that of the single-particle states, to match the AB phase acquired in each hopping by the doublon of charge $2q$:

$$|2L_\phi\rangle = \frac{1}{\sqrt{2}}\Big[|2_{1,A}\rangle - e^{i\phi}|2_{1,B}\rangle\Big] \tag{4}$$

$$|2R_\phi\rangle = \frac{1}{\sqrt{2}}\Big[|2_{L,A}\rangle - e^{-i\phi}|2_{L,B}\rangle\Big]. \tag{5}$$

Exact numerical time evolution of these states confirm their stationary nature and identifies them as eigen-

states of the Hamiltonian (2) (see Figure 3c). Photonic doublon edge states can be used to create maximally entangled multiphoton (so-called *NOON*) states, which find applications in high-precision quantum metrology. [20, 21] In our system, the state $|2L_\phi\rangle + |2R_\phi\rangle$ constitutes a NOON state. A driving potential could also be used to implement a doublon transfer protocol between both ends of the ladder, which could find applications in the field of quantum information. [16]

3.2 Bidimensional model and photonic implementation

Classical light propagating in a photonic lattice, in the paraxial approximation, follows a wave equation that can be mapped to the Schrödinger equation, and thus the amplitude of the electric field can be regarded as analogous to a wavefunction in (first quantization) quantum mechanics. To implement the Hilbert space corresponding to the two-particle 1D system, a 2D system is needed. This is a well-known method of treating the degrees of freedom in low-dimensional systems, and has been employed for both conventional [22–24] and topological materials. [18, 25].

Using the Fock basis, the Schrödinger equation for the two-particle photonic Creutz-Hubbard system, $\mathscr{H}_{CH}|\psi\rangle = E|\psi\rangle$, turns into a system of linear equations that can be interpreted as describing a single bosonic particle hopping around a quasi-2D lattice. The resulting lattice can be obtained as the Cartesian product of two Creutz ladders. The sites in this new lattice are labeled with the four indices i,α,j,β, where i,α would be the position of the first particle in the original model, and j,β that of the second one (see Figure 2a). In this way, the diagonal sites i,α,i,α correspond to states with a doubly occupied site in the original Creutz lattice. If the particle never leaves the diagonal in the 2D lattice, that implies that the corresponding 1D doublon would not decay into two separate particles. The interaction energy U has to be reinterpreted as an on-site potential in the diagonal sites of the 2D model. For the photonic lattice to correctly emulate a bosonic system, all initial states considered must be symmetric under exchange of the two particles. The exchange symmetry of the equations of motion, inherited from the simulated bosonic system, ensures a symmetric state will always remain symmetric.

Although the resulting quasi-2D lattice might be thought of as four-dimensional, the small size of two of its dimensions can be exploited to rearrange the lattice in a 3D geometry with some nonlocal hopping amplitudes, as shown in Figure 2b). To do this, it is useful to relabel the states with a new index $\zeta = 1,2,3,4$, corresponding to the values $(\alpha,\beta) = (A,A),(A,B),(B,A),(B,B)$. This small perspective shift gives the key to a possible scheme for an experimental implementation of the model. In order to construct the equivalent of a 3D lattice evolving in time in a photonic system, at least one dimension must be synthetic. In the Creutz-Hubbard model, the natural choice is the ζ dimension described above.

This is especially convenient, because synthetic gauge fields and nonlocal hopping amplitudes are easier to implement in synthetic space than real space. [26, 27] Three nonlocal hoppings would be necessary per unit cell (two for the rungless ladder), represented with dotted lines in Figure 2b. It is worth noting that, if the synthetic dimension is periodic, no nonlocal hoppings are needed. A specific setup for the photonic Creutz-Hubbard ladder could be similar to the one proposed in a recent work. [4] In it, oscillating columns of waveguides act as sites in a 2D lattice, and the synthetic dimension is represented by the modes of oscillation of the column. Four modes in a square lattice would suffice to implement our system.

In Figure 3, some two-particle numerical simulations in a $L = 6$ ladder with different parameters are represented. The plots labeled *stat.* were energy eigenstates and thus stationary. The lattice sites are arranged as indicated by Figure 2a. In an experiment, the initial state $|2_{i\alpha}\rangle$ would be easy to prepare, allowing for the observation of the different phenomena in Figure 3a.

4 Conclusions

In this work, we have studied several exotic phenomena that arise in the photonic Creutz and Creutz-Hubbard ladders. The former has already been implemented experimentally, and we propose a 3D waveguide lattice setup to implement the latter, possible thanks to the use of synthetic dimensions. It is our understanding that the current state of the art in the rapidly evolving field of photonics allows this proposal to be implemented in a real system. As far as we are aware, this would mark the first instance of a quasi-1D topological insulator with interactions in a waveguide-lattice-type quantum simulator, representing an increase in complexity compared to the strongly correlated sys-

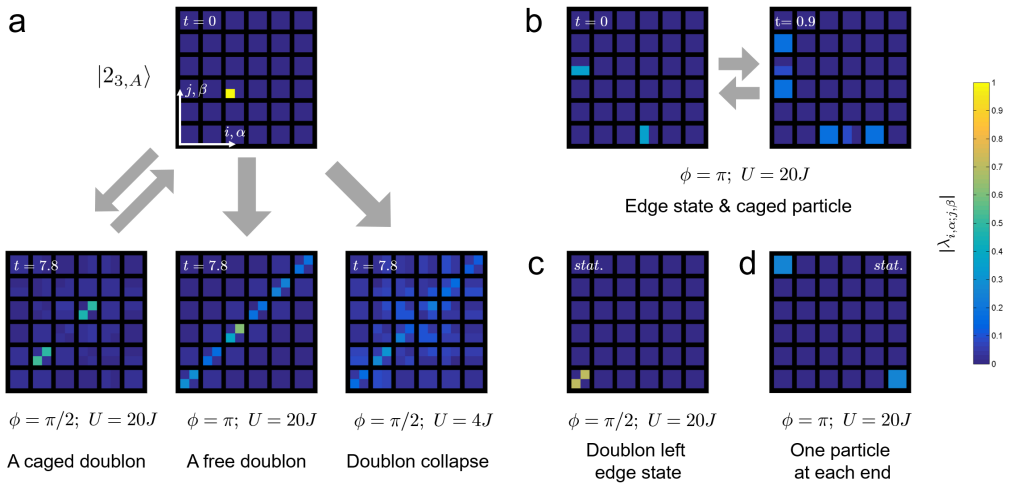

Figure 3: Two-particle time evolution simulations. a) Different time evolutions for the initial state $|2_{3,A}\rangle$, depending on the parameters of the system. b) Single particle edge state and caged particle. c) Doublon edge state. d) One particle at each end. The colorbar in the figure corresponds to the first quantization components of the wavefunction, and hence the apparent preference for the diagonal in the doublon collapse plot, which actually corresponds to a more even distribution in the Fock basis.

tems that have been implemented so far in waveguide lattices (which were both 1D and topologically trivial). [22, 24, 28–30]

We considered the two-particle model, the minimal model with interactions, and studied the doublon collapse, the different caging regimes (in particular, the doublon caging for $m = 0$, $\phi = \pi/2$) and the doublon edge states. These results show that the phase diagram of these systems have many interesting phenomena to observe away from the usually-studied $\phi = \pi$ limit. In particular, analogous caging regimes will be present for multiplons with different numbers of particles at different values of the magnetic flux, giving rise to complex physical situations that require further study.

Once realized, these photonic systems could be the first to observe many of the interesting features of the Creutz-Hubbard model, marking a milestone in the research of low-dimensional topological systems and flat band models. The Creutz and Creutz-Hubbard models constitute an ideal playground in which flat band dynamics, interactions and nontrivial topology can be studied in depth, allowing for a complete study of the rich interplay between them.

References

[1] J. Zurita, C. E. Creffield, G. Platero, *Adv. Quantum Technol.* **2019**, 1900105.
[2] R. P. Feynman, *Int. J. Theor. Phys.* **1982**, *21*, 467–488.
[3] J. Preskill, *arXiv:1203.5813*, 2012.
[4] E. Lustig, S. Weimann, Y. Plotnik, Y. Lumer, M. A. Bandres, A. Szameit, M. Segev, *Nature* **2019**, *567*(*7748*), 356–360.
[5] M. Creutz, *Phys. Rev. Lett.* **1999**, *83*, 2636–2639.
[6] L. Li, S. Chen, *Phys. Rev. B* **2015**, *92*, 085118.
[7] J. Jünemann, A. Piga, S.-J. Ran, M. Lewenstein, M. Rizzi, A. Bermudez, *Phys. Rev. X* **2017**, *7*, 031057.
[8] D. Sticlet, L. Seabra, F. Pollmann, J. Cayssol, *Phys. Rev. B* **2014**, *89*, 115430.
[9] Y. Kuno, T. Orito, I. Ichinose, *arXiv:1904.03463*, 2019.
[10] M. Tovmasyan, S. Peotta, P. Törmä, S. D. Huber, *Phys. Rev. B* **2016**, *94*, 245149.
[11] M. Tovmasyan, S. Peotta, L. Liang, P. Törmä, S. D. Huber, *Phys. Rev. B* **2018**, *98*, 134513.
[12] S. Takayoshi, H. Katsura, N. Watanabe, H. Aoki, *Phys. Rev. A* **2013**, *88*, 063613.
[13] M. Tovmasyan, E. P. L. van Nieuwenburg, S. D. Huber, *Phys. Rev. B* **2013**, *88*, 220510.
[14] S. Bravyi, D. P. DiVincenzo, D. Loss, *Ann. Phys.* **2011**, *326*(*10*), 2793–2826.
[15] F. Hofmann, M. Potthoff, *Phys. Rev. B* **2012**, *85*, 205127.
[16] M. Bello, C. E. Creffield, G. Platero, *Sci. Rep.* **2016**, *6*, 22562.
[17] M. Bello, C. E. Creffield, G. Platero, *Phys. Rev. B* **2017**, *95*, 094303.
[18] M. A. Gorlach, A. N. Poddubny, *Phys. Rev. A* **2017**, *95*, 053866.
[19] G. Salerno, M. Di Liberto, C. Menotti, I. Carusotto, *Phys. Rev. A* **2018**, *97*, 013637.
[20] I. Afek, O. Ambar, Y. Silberberg, *Science* **2010**, *328*(*5980*), 879–881.
[21] M. A. Gorlach, A. N. Poddubny, *Phys. Rev. A* **2017**, *95*, 033831.
[22] S. Longhi, *Opt. Lett.* **2011**, *36*(*16*), 3248–3250.
[23] S. Longhi, G. D. Valle, *Opt. Lett.* **2011**, *36*(*24*), 4743–4745.
[24] S. Mukherjee, M. Valiente, N. Goldman, A. Spracklen, E. Andersson, P. Öhberg, R. R. Thomson, *Phys. Rev. A* **2016**, *94*, 053853.
[25] M. Di Liberto, A. Recati, I. Carusotto, C. Menotti, *Phys. Rev. A* **2016**, *94*, 062704.
[26] B. A. Bell, K. Wang, A. S. Solntsev, D. N. Neshev, A. A. Sukhorukov, B. J. Eggleton, *Optica* **2017**, *4*(*11*), 1433–1436.
[27] L. Yuan, Q. Lin, M. Xiao, S. Fan, *Optica* **2018**, *5*(*11*), 1396–1405.
[28] D. O. Krimer, R. Khomeriki, *Phys. Rev. A* **2011**, *84*, 041807.
[29] G. Corrielli, A. Crespi, G. Della Valle, S. Longhi, R. Osellame, *Nat. Commun.* **2013**, *4*(*1*).
[30] A. Rai, C. Lee, C. Noh, D. G. Angelakis, *Sci. Rep.* **2015**, *5*, 8438.